A theoretical solution of resonant circular diaphragm-type piezoactuators with added mass loads

Yuanlin Hu · Xin Liang · Wen Wang[1]

Abstract: A theoretical solution is formulated to analyze the vibration behaviors of circular diaphragm-type piezoactuators based on the Hamilton's principle and Rayleigh-Ritz method, which are particular suitable for modeling the deflection of multilayer structures. Each of the actuator three layers is considered as an individual layer in the modeling. The energy associated with the solution includes the kinetic energy of the actuator, the elastic potential energy of the various layers, the electric potential energy in the piezodisc, and the work done by the force of electric filed. The transverse displacement is separated into a time dependence term and a mode shape term, then the vibrational governing equation is derived using the functional variation, and is approximately solved through the method of multiple scales. Moreover, added mass loads are introduced to the diaphragm center for the sake of decreasing the resonant frequency, where many MEMS devices, such as gas micropumps and ejectors, have a higher working efficiency. The proposed analytical solution is validated numerically via the finite element method (FEM) and experimentally via measurements; the theoretical results are found to be in good agreement with the FEM results as well as with the experimental results. Furthermore, the effects of mass loads, geometric dimensions and material properties of the piezoactuator on the resonant frequency are discussed.

Key words: piezoelectric actuators; resonant frequency; Hamilton's principle; mass loads; MEMS

1 Introduction

The multilayer diaphragm-type piezoactuators, converting electrical energies into mechanical ones, are extensively applied to the micro electro mechanical systems (MEMS), such as complex fluidic handing systems consisting micropumps [1], ejectors [2], drug deliveries [3], and etc. Normally, a diaphragm-type piezoactuator is composed of passive layer, bonding layer and PZT layer, shown in Fig. 1(a). When a voltage is imposed on the piezodisc, its contraction or expansion in the radial and lateral directions induces a bending moment to the actuator, and results in a deformation in transverse direction. Such actuators with a piece of piezodisc bonded on one side or both sides of the passive layer are termed as unimorph or bimorph, respectively. Furthermore, in most applications, the radii of the piezoelectric and bonding layers are generally smaller than the radius of the passive layer to generate larger deflections, and the piezoactuator is tightly clamped around its periphery [4].

Accurate analytical solution to the deflections of such diaphragm-type piezoactuators in terms of the actuator dimensions, material properties, and loads are highly valuable for their design. The static analysis is appropriate when the excitation frequency of the piezoactuator is considerably below its resonant frequency. However, the static deflections of these piezoactuators are mostly less than 0.5 μm/V [5, 6], which limits the developments of various piezoelectric

devices and is desired to be enhanced for a higher working efficiency. Taking the piezoactuated gas micropumps as an instance, larger deflection of the actuator is much helpful in promoting the pressure rise and flow rate [7]. According to the vibration theory, an effective method to amplify the deflection is exciting the actuator at its resonant frequency. Therefore, theoretical solution on the resonant analysis of the diaphragm-type piezoactuators is necessary.

The vibration behaviors of the diaphragm-type piezoactuators have attracted many attentions in the past decades because of their important role in MEMS devices. The investigations include analytical solutions [8], finite element method (FEM) simulations [9] and experimental measurements [10]. For the computational efforts, classic plate theory (CPT), which based on the Kirchhoff plate model, has been widely employed to study free vibration of the piezoelectric thin circular/annular plates. Based on the CPT, a research was conducted by Wang et al. [11] on analytical solution for free vibration behaviors of a piezoelectric coupled circular plate with simply supported and clamped boundary conditions; the solution was validated through the FEM simulation. Duan et al. [12] investigated free vibration behaviors of a piezoelectric coupled thick annular plate based on the Kirchhoff and Mindlin plate theories, and the results indicated that thicker PZT layer increases the resonant frequency of the actuator. Compared with the piezoelectric coupled thick plates, thin diaphragm-type piezoactuators always have larger transverse displacements and lower resonant frequencies [13], and are suitable for the fluidic handling systems. Yao et al. [14] investigated dynamic behaviors of a square edge-clamped multilayer piezoelectric diaphragm based on the CPT and obtained the governing differential equations using the Rayleigh-Ritz method. They concluded that the density and elastic modulus of the actuator are dominant factors affecting the resonant frequency of the actuator through the parametric study. Employing the Hamilton's principle, dynamic behaviors of a one side clamped rectangular piezoelectric actuator were studied by Zhao et al. [15], using the first-order shear deformation theory to model the thick laminated plate. Olfatnia et al. [16] investigated the vibrational characteristics of a circular piezoactuator used for the biosensors after introducing the residual stress of the diaphragm to the governing equation, supposing the multilayer diaphragm as one membrane. They also observed the vibration modes of the circular diaphragm through a microscope, suggesting that the first mode had the maximum energy emission to the medium [17]. Gomes [18] proposed a new theory on the vibration of a circular piezoelectric diaphragm with an approach to separate the diaphragm into an inner circular multilayer membrane and an outer annular elastic membrane, which generated two distinct eigenvalues. After considering the damping and relaxed clamping conditions of the diaphragm, overestimation of the resonant frequency was explained and the theory agreed well with the experimental measurements. Such piezoactuators utilized in the micropump were also investigated by Kaviani [19], who derived a dynamic model through explicitly solving the governing equations using separation of variables method; the damping effect was considered and the theory was verified by the FEM simulation. Using the piezoelectric constitutive equations, Esfahani and Bahrami [20] proposed governing equations to investigate the vibration behaviors of an edge-clamped piezoelectric micro-plate in fluidic environment, which was modeled as a damping foundation. The equations were solved using generalized differential quadrature method and were also validated through FEM simulation. Based on the thin plate theory and Kelvin–Voigt laws, another work concerning the vibration of a piezoelectric microplate was also presented by Esfahani and Bahrami [21].

The resonant frequencies of the circular piezoactuators utilized in the transducers are mostly over 10 kHz. However, the frequency at that range is too high for the fluidic handling devices and may results in a failure. Such as in the micropumps, higher excitation frequency is benefit for the power output of the piezodisc, but too high working frequency may lead to the failure of the mechanical valves [22]. Moreover, too high working frequency may causes tremendous energy loss due to the acoustic radiation [23]. One effective method to drop the resonant frequency of the diaphragm without weakening the actuation force is fixing an added mass load at the diaphragm center, which has been frequently utilized in the piezoelectric energy harvesting devices [24].

A previous method to model the vibrational diaphragm piezoactuators was via eigenvalue analysis to the mode function. However, the multilayer actuator was supposed as one membrane for the method, which may result in discrepancies. Moreover, the mode function may difficult to be solved when some other terms, such as mass load, are introduced to the governing equations.

This research presents an analytical solution on the dynamic behaviors of a circular diaphragm-type piezoactuator based on the Hamilton's principle and the Rayleigh-Ritz method. Deflection of the actuator satisfies the Kirchhoff thin plate theory. The Energy associated with the solution includes the elastic potential energy of the deflecting actuator, the kinetic energy during the vibration, the electric potential energy in the piezodisc, and the work done by the force of electric filed. Each of the piezoactuator three layers is considered as an individual layer in the

dynamic modeling. Moreover, a mass load is incorporated to the actuator for the purpose of decreasing its resonant frequency. The proposed solution is validated via the FEM simulation as well as the experimental measurement. Based on the equations, effects of the center mass load, actuator dimensions, and material properties of the passive layer on the piezoactuator resonant frequency are further investigated.

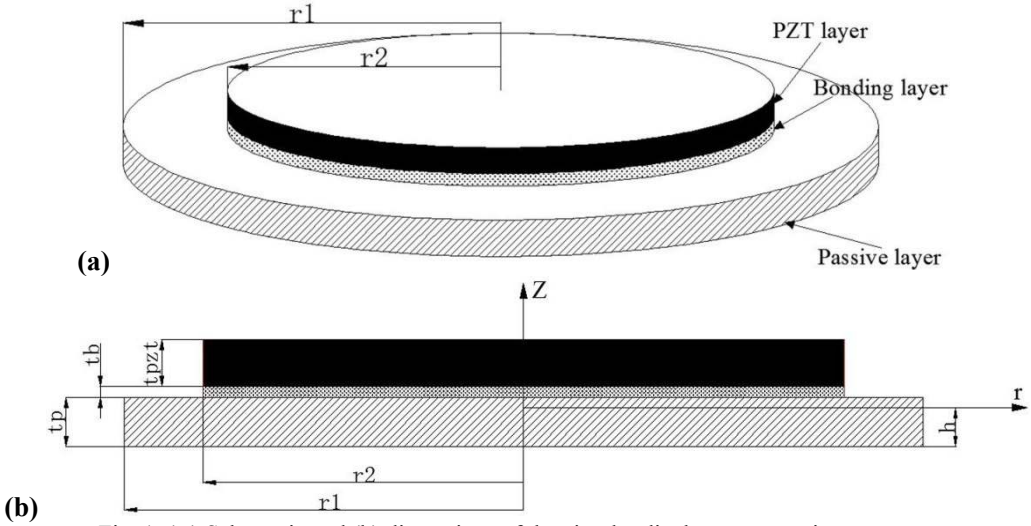

Fig. 1. (a) Schematic and (b) dimensions of the circular diaphragm-type piezoactuator

2 Analytical modeling

The basic idea of the multilayer diaphragm-type piezoactuators is converting the contraction or expansion of the PZT layer in radial and lateral directions to a large bending displacement of the actuator in the transverse direction, and the conversion is fulfilled through the bonding layer, which tightly glues the passive layer and PZT layer together. As presented in Fig. 1(b), the radius of the PZT layer and bonding layer is r_2, and the radius of the passive layer is r_1; the thicknesses of the passive layer, bonding layer and PZT layer are t_p, t_b, and t_{pzt}, where the subscript p, b, and pzt represent the passive layer, the bonding layer, and the PZT layer, respectively. In the multilayer structure, there exists a neutral plane that has no transverse strain, and h is the distance from the neutral plane to the bottom of the passive layer. The actuator vibrates with a fixed periphery. The modeling is based on the following assumptions:

(1) Isotropic multilayer diaphragm and uniformly distributed properties; the PZT layer is polarized along z direction.
(2) The deflection follows the Kirchhoff thin plate theory: (i) the normal stress and shear stress are neglected, i.e. $\sigma_{zz}=0$; (ii) elements remain perpendicular to the neutral surface after bending, i.e. $e_{rz}=e_{\theta z}=0$.
(3) Impact of the electrodes layer on the deflection is neglected since its thickness is less than 0.5 μm [25]; the viscoelastic nature of the bonding layer is neglected [26].
(4) Electric potential is assumed to be evenly distributed along the thickness of the PZT layer.

2.1 Governing equations of the piezoactuator

The stains and stresses in both radial and lateral directions are considered in the three layers. Based on the Kirchhoff thin plate theory, radial displacement (u_r), lateral displacement (u_θ), radial strain (e_{rr}) and lateral strain ($e_{\theta\theta}$) of the actuator are defined [27]:

$$\begin{cases} u_r = -z\dfrac{\partial w}{\partial r} \\ u_\theta = -z\dfrac{\partial w}{r\partial r} \end{cases} \tag{1}$$

$$\begin{cases} e_{rr} = \dfrac{\partial u_r}{\partial r} = -z\dfrac{d^2 w}{dr^2} \\ e_{\theta\theta} = \dfrac{u_r}{r} = -z\dfrac{dw}{rdr} \end{cases} \tag{2}$$

where w represents the transverse displacement and is a function of r, θ and t.

According to the generalized Hook's Law, stresses in radial ($\sigma_{rr,p}$) and lateral ($\sigma_{\theta\theta,p}$) directions of the passive layer are calculated as

$$\begin{cases} \sigma_{rr,p} = \dfrac{E_p}{1-\upsilon_p^2}\left(e_{rr} + \upsilon_p e_{\theta\theta}\right) = -\dfrac{zE_p}{1-\upsilon_p^2}\left(\dfrac{d^2w}{dr^2} + \dfrac{\upsilon_p}{r}\dfrac{dw}{dr}\right) \\ \sigma_{\theta\theta,p} = \dfrac{E_p}{1-\upsilon_p^2}\left(e_{\theta\theta} + \upsilon_p e_{rr}\right) = -\dfrac{zE_p}{1-\upsilon_p^2}\left(\upsilon_p\dfrac{d^2w}{dr^2} + \dfrac{dw}{rdr}\right) \end{cases} \tag{3}$$

where E_p and v_p are the Young's modulus and Poisson's ratio of the passive layer.

The thickness of the bonding layer is around 20 μm, which is far thinner than the passive layer and PZT layer, its viscoelastic nature is negligible. Hence, the stresses in radial ($\sigma_{rr,b}$) and lateral ($\sigma_{\theta\theta,b}$) directions of the bonding layer are expressed as

$$\begin{cases} \sigma_{rr,b} = \dfrac{E_b}{1-\upsilon_b^2}\left(e_{rr} + \upsilon_b e_{\theta\theta}\right) = -\dfrac{zE_b}{1-\upsilon_b^2}\left(\dfrac{d^2w}{dr^2} + \dfrac{\upsilon_b}{r}\dfrac{dw}{dr}\right) \\ \sigma_{\theta\theta,b} = \dfrac{E_b}{1-\upsilon_b^2}\left(e_{\theta\theta} + \upsilon_b e_{rr}\right) = -\dfrac{zE_b}{1-\upsilon_b^2}\left(\upsilon_b\dfrac{d^2w}{dr^2} + \dfrac{dw}{rdr}\right) \end{cases} \tag{4}$$

According to the linear piezoelectric constitutive equations, stresses in radial ($\sigma_{rr,b}$) and lateral ($\sigma_{\theta\theta,b}$) directions of the PZT layer are calculated as

$$\begin{cases} \sigma_{rr,pzt} = \dfrac{1}{s_{11}^E\left(1-\upsilon_{pzt}^2\right)}\left(e_{rr} + \upsilon_{pzt} e_{\theta\theta}\right) - \dfrac{d_{31}}{s_{11}^E\left(1-\upsilon_{pzt}\right)}E_Z \\ \sigma_{\theta\theta,pzt} = \dfrac{1}{s_{11}^E\left(1-\upsilon_{pzt}^2\right)}\left(e_{\theta\theta} + \upsilon_{pzt} e_{rr}\right) - \dfrac{d_{31}}{s_{11}^E\left(1-\upsilon_{pzt}\right)}E_Z \end{cases} \tag{5}$$

where E_z is the electrical field strength in the PZT layer.

2.2 Theory of vibration

Based on the generalized Hamilton's principle, the variational function of the piezoactuator is expressed as [28]

$$\delta F = \int_{t_1}^{t_2}\delta\left(T - U + W_e\right)dt + \int_{t_1}^{t_2}\delta W dt = 0 \tag{6}$$

where F is a function of time; T, U and W_e are the kinetic energy, potential energy and electric energy of the actuator, respectively. W is the work done by the force of electric field. For the multilayer piezoactuator, they are expressed as

$$\begin{cases} T = \displaystyle\int_V \frac{1}{2}\rho v v^T dV \\ U = \displaystyle\int_V \frac{1}{2}\sigma\varepsilon^T dV \\ W_e = \displaystyle\int_{V_{pzt}} \frac{1}{2}D_z E_z dV \\ \delta W = -q(t)\delta V(t) \end{cases} \tag{7}$$

where v is the velocity of the actuator and satisfies: $v = \partial w / \partial t$; σ and ε are the strain and stress of the layers, D_z is the electric displacement of the PZT layer, $V(t)$ is the excitation voltage imposed on the PZT layer, and $q(t)$ is the charge on the surface of the PZT layer.

When a mass is fixed at the diaphragm center, shown in Fig. 2, the kinetic energy (T) of the piezoactuator is comprised of the kinetic energy of the three layers and the mass (T_m). Therefore, the total kinetic energy (T) and total elastic potential energy (U) of the actuator is

$$\begin{cases} T = T_p + T_b + T_{pzt} + T_m \\ U = U_p + U_b + U_{pzt} \end{cases} \tag{8}$$

The Rayleigh-Ritz method is one of the methods solving boundary value problems through reformulating the given problems to a minimization problem [15]. To obtain the governing equations based on the method, separating the displacement (w) as

$$w(r,\theta,t) = \phi(r,\theta)\cdot X(t) \tag{9}$$

where $\phi(r,\theta)$ is the vibration function describing shape of the actuator at resonance, and $X(t)$ is

the displacement mode.

Substituting the Eq. (9) into (8), the expressions of kinetic energy and elastic potential energy of the actuator are reformulated; hence the total kinetic energy (T) of the three layers is expressed as

$$\begin{cases} T = \frac{1}{2}\left(\int_{V_p} \rho_p \upsilon\upsilon^T dV + \int_{V_b} \rho_b \upsilon\upsilon^T dV + \int_{V_{pzt}} \rho_{pzt} \upsilon\upsilon^T dV + \int_{V_m} \rho_m \upsilon\upsilon^T dV \right) = M\left(\frac{dX(t)}{dt} \right)^2 \\ M = \frac{1}{2}\left(\int_{V_p} \rho_p \phi^2 dV + \int_{V_b} \rho_b \phi^2 dV + \int_{V_{pzt}} \rho_{pzt} \phi^2 dV + \int_{V_m} \rho_m \phi^2 dV \right) \end{cases} \tag{10}$$

Likewise, total elastic potential energy (U) of the three layers is expressed as

$$U = U_p + U_b + U_{pzt} = KX^2(t) + K_1 X^2(t) E_z + K_2 X(t) E_z \tag{11}$$

where U_p, U_b and U_{pzt} are the elastic potential energy for each layer calculated through Eq. (12); K, K_1 and K_2 are expressed as Eq. (13).

$$\begin{cases} U_p = \int_{V_p} \frac{1}{2}(\sigma_{rr,p} e_{rr,p} + \sigma_{\theta\theta,p} e_{\theta\theta,p}) dV \\ \quad = \frac{E_p}{2(1-v_p^2)} \int_{V_p} z^2 \left[\left(\frac{d^2\phi}{dr^2} \right)^2 + 2\frac{v_p}{r}\left(\frac{d^2\phi}{dr^2} \right)\left(\frac{d\phi}{dr} \right) + \frac{1}{r^2}\left(\frac{d\phi}{dr} \right)^2 \right] dV \cdot X^2(t) \\ U_b = \int_{V_b} \frac{1}{2}(\sigma_{rr,b} e_{rr,b} + \sigma_{\theta\theta,b} e_{\theta\theta,b}) dV \\ \quad = \frac{E_p}{2(1-v_b^2)} \int_{V_b} z^2 \left[\left(\frac{d^2\phi}{dr^2} \right)^2 + 2\frac{v_b}{r}\left(\frac{d^2\phi}{dr^2} \right)\left(\frac{d\phi}{dr} \right) + \frac{1}{r^2}\left(\frac{d\phi}{dr} \right)^2 \right] dV \cdot X^2(t) \\ U_{pzt} = \int_{V_{PZT}} \frac{1}{2}(\sigma_{rr,pzt} e_{rr,pzt} + \sigma_{\theta\theta,p} e_{\theta\theta,pzt}) dV \\ \quad = \int_{V_{pzt}} \frac{z^2}{2s_{11}^E(1-v_{pzt}^2)} \left[\left(\frac{d^2\phi}{dr^2} \right)^2 + 2\frac{v_b}{r}\left(\frac{d^2\phi}{dr^2} \right)\left(\frac{d\phi}{dr} \right) + \frac{1}{r^2}\left(\frac{d\phi}{dr} \right)^2 \right] dV \cdot X^2(t) \\ \quad + \int_{V_{pzt}} \frac{d_{31} z}{2s_{11}^E(1-v_{pzt})} \left(\frac{d^2\phi}{dr^2} \right) dV \cdot X^2(t) \cdot E_z + \int_{V_{pzt}} \frac{d_{31} z}{2s_{11}^E(1-v_{pzt})} \left(\frac{d\phi}{rdr} \right) dV \cdot X(t) \cdot E_z \end{cases} \tag{12}$$

$$\begin{cases} K = \frac{E_p}{2(1-v_p^2)} \int_{V_p} z^2 \left[\left(\frac{d^2\phi}{dr^2} \right)^2 + 2\frac{v_p}{r}\left(\frac{d^2\phi}{dr^2} \right)\left(\frac{d\phi}{dr} \right) + \frac{1}{r^2}\left(\frac{d\phi}{dr} \right)^2 \right] dV \\ \quad + \frac{E_b}{2(1-v_b^2)} \int_{V_b} z^2 \left[\left(\frac{d^2\phi}{dr^2} \right)^2 + 2\frac{v_b}{r}\left(\frac{d^2\phi}{dr^2} \right)\left(\frac{d\phi}{dr} \right) + \frac{1}{r^2}\left(\frac{d\phi}{dr} \right)^2 \right] dV \\ \quad + \frac{1}{2s_{11}^E(1-v_{pzt}^2)} \int_{V_{pzt}} z^2 \left[\left(\frac{d^2\phi}{dr^2} \right)^2 + 2\frac{v_{pzt}}{r}\left(\frac{d^2\phi}{dr^2} \right)\left(\frac{d\phi}{dr} \right) + \frac{1}{r^2}\left(\frac{d\phi}{dr} \right)^2 \right] dV \\ K_1 = \int_{V_{pzt}} \frac{d_{31} z}{2s_{11}^E(1-v_{pzt})} \left(\frac{d^2\phi}{dr^2} \right) dV \\ K_2 = \int_{V_{pzt}} \frac{d_{31} z}{2s_{11}^E(1-v_{pzt})} \left(\frac{d\phi}{rdr} \right) dV \end{cases} \tag{13}$$

The electric potential energy (W_e) in the PZT layer is reformulated as

$$\begin{cases} W_e = \int_{V_{pzt}} \frac{1}{2} D E_z{}^T dV = \frac{1}{2} \int_{V_{pzt}} \left(d_{31}(\sigma_{rr,pzt} + \sigma_{\theta\theta,pzt}) + \varepsilon_{33} E_z \right) E_z dV = F E_z{}^2 - F_1 X(t) E_z \\ F = \frac{1}{2} \int_{V_{pzt}} \left(\varepsilon_{33} - \frac{2 d_{31}^2}{s_{11}^E (1 - \upsilon_{pzt})} \right) dV \\ F_1 = \frac{1}{2} \int_{V_{pzt}} \frac{z d_{31}}{s_{11}^E (1 - \upsilon_{pzt})} \left(\frac{d^2 \phi}{dr^2} + \frac{1}{r} \frac{d\phi}{dr} \right) dV \end{cases} \tag{14}$$

According to the Kirchhoff thin plate theory, there is a neutral plane that has no transverse strain in the multilayer structure, and the volume integration of each layer is relates to its location, which influences the diaphragm deformation. The volume integration of each layer is expressed as

$$\begin{cases} \int_{V_p} dV = \int_0^{2\pi} \int_0^{r_1} \int_{-h}^{t_p - h} r dr d\theta dz \\ \int_{V_b} dV = \int_0^{2\pi} \int_0^{r_2} \int_{t_p - h}^{t_b + t_p - h} r dr d\theta dz \\ \int_{V_{pzt}} dV = \int_0^{2\pi} \int_0^{r_2} \int_{t_b + t_p - h}^{t_{pzt} + t_b + t_p - h} r dr d\theta dz \end{cases} \tag{15}$$

where h is the distance from the neutral plane to the bottom of the passive layer, and can be obtained based on the moment balance,

$$\int_0^{t_p - h} \frac{E_p}{1 - v_p^2} z dz + \int_{t_p - h}^{t_p - h + t_b} \frac{E_b}{1 - v_b^2} z dz + \int_{t_p - h + t_b}^{t_p - h + t_b + t_{pzt}} \frac{1}{s_{11}^E (1 - v_{pzt}^2)} z dz = 0 \tag{16}$$

Li and Chen [6] has approximately computed the neutral plane for the unimorph piezoactuator as

$$h = \frac{1}{2} \frac{E_p t_p^2 / (1 - u_p^2) + E_b \left[(t_b + t_p)^2 - t_p^2 \right] / (1 - u_b^2) + \left[(t_{pzt} + t_b + t_p)^2 - (t_b + t_p)^2 \right] / s_{11}^E (1 - v_{pzt}^2)}{E_p t_p / (1 - v_p^2) + E_b t_b / (1 - v_b^2) + t_{pzt} / \left[s_{11}^E (1 - v_p^2) \right]} \tag{17}$$

The electric potential (φ) of the piezoelectric layer is usually supposed evenly distributed, thus the electric field strength (E_z) is calculated as

$$E_z(t) = -\frac{d\varphi}{dz} = \frac{V(t)}{t_{pzt}} \tag{18}$$

Substituting Eqs. (10), (11) and (14) into (6) results in

$$\begin{aligned} 0 &= \int_{t_1}^{t_2} \delta (T - U + W_e) dt + \int_{t_1}^{t_2} \delta (W) dt \\ &= \int_{t_1}^{t_2} \delta \left(M \left(\frac{dX(t)}{dt} \right)^2 \right) dt - \int_{t_1}^{t_2} \delta \left(K X(t)^2 + K_1 X^2(t) E(t) + K_2 X(t) E(t) \right) dt \\ &\quad + \int_{t_1}^{t_2} \delta \left(F V^2(t) - F_1 X(t) E(t) \right) dt - \int_{t_1}^{t_2} 2 q(t) \cdot \delta V(t) dt \end{aligned} \tag{19}$$

According to the variational principle, the functional derivative of $X(t)$ is equal to zero, therefore governing equation concerning the vibrational piezoactuator is obtained. In order to prevent infinite deflections when the actuator is excited at its resonant frequency, the governing equation needs to account for the damping effect. After introducing the damping coefficient (C), the governing equation is expressed as

$$\frac{d^2 X(t)}{dt^2} + \frac{C}{M} \frac{dX(t)}{dt} + \frac{K}{M} X(t) = -\frac{K_1}{M} X(t) E_z(t) - \frac{K_2 + F_1}{2M} E_z(t) \tag{20}$$

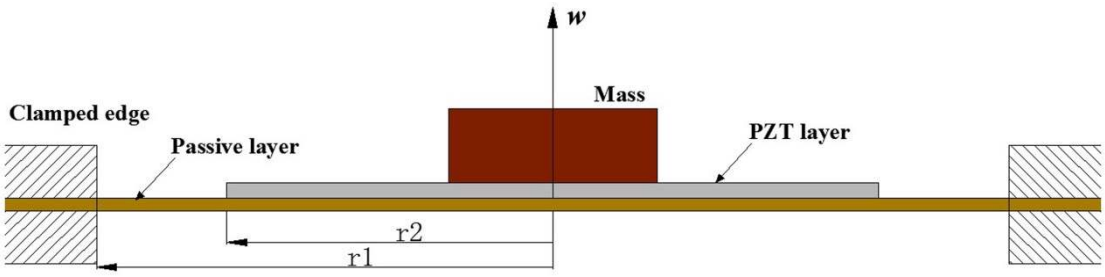

Fig. 2. The schematic of the piezoactuator with a mass load

2.3 The primary resonance

Introducing several none-dimensional variables: $E(t) = -\frac{V_0}{t_{pzt}}\cos(\omega t)$, $\tau = \sqrt{\frac{K}{M}} \cdot t = \omega_n \cdot t$, where ω is the frequency of the excitation signal. The Eq. (20) is rewritten as

$$X''(\tau) + \mu X'(\tau) + X(\tau) = fX(\tau)\cos(\lambda\tau) + f_1\cos(\lambda\tau) \tag{21}$$

where $\mu = \frac{C}{\sqrt{MK}}$, $f = \frac{K_1}{t_{pzt}K}V_0$, $f_1 = \frac{K_2 + F_1}{2Kt_{pzt}}V_0$, $\lambda = \frac{\omega}{\omega_n}$.

To analyze the primary fundamental resonance, the λ can be expressed as,

$$\lambda = 1 + \varepsilon\theta \tag{22}$$

where θ is the detuning factor that describes the nearness of the excitation frequency to the resonant frequency; when $\theta=0$, the resonance occurs and the nonlinear force and external force are small variables compared with the inertial force and linear force, therefore a small parameter ε is introduced to the Eq. (21), resulting in

$$X''(\tau) + \mu X'(\tau) = \varepsilon\left(-X(\tau) + fX(\tau)\cos(\lambda\tau) + f_1\cos(\lambda\tau)\right) \tag{23}$$

The method of multiple scales is utilized to solve Eq. (23), and the first-order approximation is mainly considered [29]. Thus, $X(\tau)$ is expanded as,

$$X(\tau) = X_0(T_0, T_1) + \varepsilon X_1(T_0, T_1) \tag{24}$$

Substituting Eq. (24) into (23) results in

$$\begin{cases} D_0^2 X_0 + X_0 = 0 \\ D_0^2 X_1 + X_1 = -2D_0D_1X_0 - \mu D_0X_0 + fX_0\cos(T_0 + \theta T_1) + f_1\cos(T_0 + \theta T_1) \end{cases} \tag{25}$$

where $D_i = \partial/\partial T_i, (i = 0,1)$.

The solution of Eq. (25) is,

$$D_0^2 R_1 + R_1 = \left(-2iD_1A - \mu iA + \frac{f_1}{2}e^{i\theta T_1}\right)\cdot e^{iT_0} + \frac{f}{2}e^{i\theta T_1}\left(Ae^{2iT_0} + \bar{A}\right) + cc \tag{26}$$

where $A = \frac{a(T_1)}{2}e^{i\beta(T_1)}$, $a(T_1)$ is the amplitude, $\beta(T_1)$ is the phase, $\bar{A}$ is the conjugate of the A, and cc is the conjugate of the frontal terms.

To eliminating the secular terms,

$$-2iD_1A - \mu iA + \frac{f_1}{2}e^{i\theta T_1} = 0 \tag{27}$$

For the steady solution: $D_1a = 0$, $D_1\varphi = 0$, where $\varphi = \theta T_1 - \beta(T_1)$. Separating the real part and imaginary part of Eq. (26), the amplitude and the phase of the resonant actuator are obtained,

$$\begin{cases} -\frac{1}{2}\mu a + \frac{f_1}{2}\sin\varphi = 0 \\ \theta a + \frac{f_1}{2}\cos\varphi = 0 \end{cases} \tag{28}$$

For the edge-clamped circular piezoactuator, its vibration function (ϕ) satisfies the boundary conditions as follows,

$$w\big|_{r=r_1}=0,\quad \left.\frac{dw}{dr}\right|_{r=r_1}=0,\quad \frac{\partial w}{\partial\theta}=0 \tag{29}$$

Therefore, the vibration function at the resonance can be expanded in the form of power series, shown as

$$\begin{cases}\phi(r)=\left(1-\dfrac{r^2}{r_1^2}\right)^2\left[\displaystyle\sum_{i=1}^{n}a_i\left(1-\frac{r^2}{r_1^2}\right)^{i-1}+R(n)\right]\\ R(n)=\dfrac{\left(1-r^2/r_1^2\right)^{n+1}}{(n+1)!}\phi^{(n+1)}(\xi)\end{cases} \tag{30}$$

where *R(n)* is the remainder term of the series. According to the Rayleigh-Ritz method, the constants a_i in the power series are determined by equations: $\partial L/\partial a_i=0$, $(i=1,2,3,...,n)$, where *L* is the static potential energy of the piezoactuator expressed as: $L=U_p+U_b+U_{pzt}-W_E$. Moreover, the $\phi(r)$ is investigated with different degrees (*n*), and the shape is stable when $n\geq 3$; we take $n=4$ in the analytical solution.

3 Validation of the analytical solution

The analytical solution on dynamic behaviors of the circular diaphragm-type piezoactuator was validated via both FEM simulations and experimental measurements. Three types of piezoactuators with different thicknesses were simulated in ANSYS and measured through a laser displacement sensor. Their geometric dimensions and material properties were summarized in Table 1 and 2, respectively. Furthermore, to investigate the effects of the added mass load, a cylinder mass was bonded at each piezoactuator center, and they were simulated and measured as well. The radius of the cylinder mass was 5 mm, and various weights were fulfilled through changing the height. Deduced from the experimental measurements, the average coefficient of damping ratio (μ) was 0.032 for the three piezoactuators without a center mass, and was 0.027 for the three piezoactuators with a center mass of 3.6 g.

Table 1 Dimensions of the three multilayer piezoactuators

Layers	Dimensions (radius×thickness)		
	Type A (*t*=0.24 mm)	Type B (*t*=0.36 mm)	Type C (*t*=0.48 mm)
PZT layer	12.5 mm×120 μm	12.5 mm×180 μm	12.5 mm×240 μm
Bonding layer	12.5 mm×20 μm	12.5 mm×20 μm	12.5 mm×20 μm
Passive layer	17.5 mm×100 μm	17.5 mm×160 μm	17.5 mm×220 μm

Table 2 Material properties of the three multilayer piezoactuators

Layer	Mechanical properties	Value
PZT layer (PZT-5A)	Piezoelectricity ***e*** (C/m)	$\begin{bmatrix}0&0&-5.4\\0&0&-5.4\\0&0&15.8\\0&12.3&0\\12.3&0&0\\0&0&0\end{bmatrix}$
	Permittivity (F/m)	$\begin{bmatrix}8.107&0&0\\0&8.107&0\\0&0&7.346\end{bmatrix}\times10^{-9}$

	Compliance $\boldsymbol{S}$ (m^2/N)	$\begin{bmatrix} 16.4 & -5.75 & -8.45 & 0 & 0 & 0 \\ -5.75 & 16.4 & -8.45 & 0 & 0 & 0 \\ -8.45 & -8.45 & 18.8 & 0 & 0 & 0 \\ 0 & 0 & 0 & 44.3 & 0 & 0 \\ 0 & 0 & 0 & 0 & 47.5 & 0 \\ 0 & 0 & 0 & 0 & 0 & 47.5 \end{bmatrix} \times 10^{-12}$
Passive layer (Brass)	Density (kg/m^3)	7500
	Elastic modulus (GPa)	100
	Poisson's ratio	0.27
Bonding layer (Epoxy resin)	Density (kg/m^3)	9500
	Elastic modulus (GPa)	5.17
	Poisson's ratio	0.3
	Density (kg/m^3)	2000

3.1 Harmonic analysis through FEM simulations

The harmonic analysis to the three types of piezoactuators both with and without a mass of 3.6 g at their center was done with ANSYS. The coupled-field element Solid-226 with 20 nodes was chosen to model the PZT layer; the solid element Solid-186 with 20 nodes was chosen to model the brass layer, the epoxy resin layer and the center mass. The periphery of the passive layer was fixed, consistent with the boundary conditions for the analytical solution. The sinusoidal actuation voltage was imposed on the nodes belong to the upper and lower surfaces of the PZT layer. The actuation voltage kept constant at 20 V_{pp} with frequencies varying in steps of 2 Hz. The dimensions and the material properties of the actuators simulated in the finite element model were the same as those of the tested actuators given in Table 1 and 2.

(a)

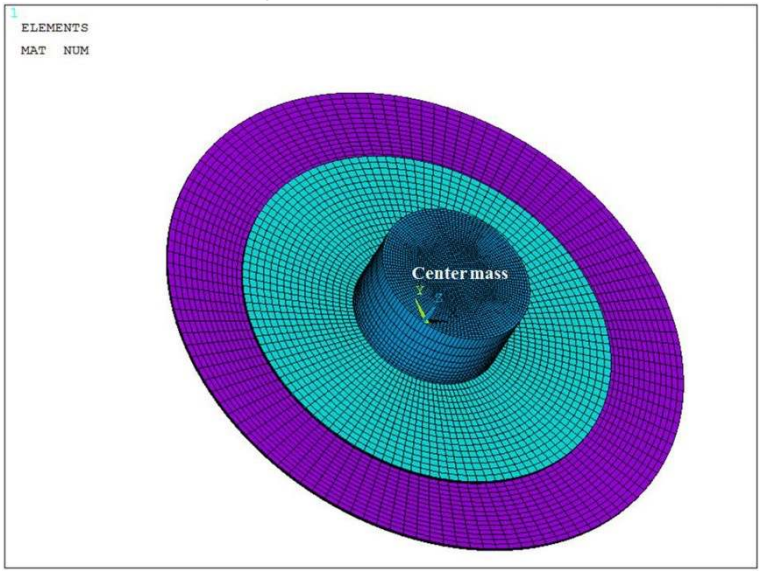

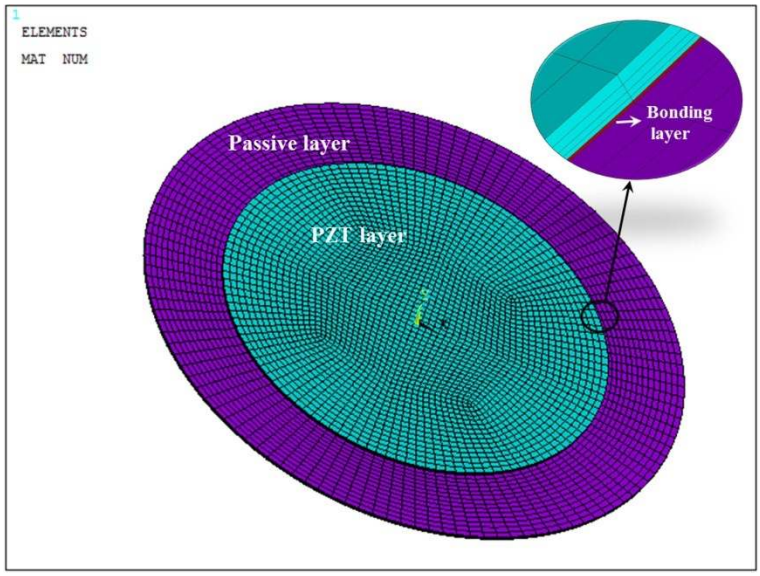

(b)

Fig. 3. Elements plot of the piezoactuator (a) with and (b) without center mass

According to the grid independence examination, over 28000 elements (3 division of the minimum length) are required to obtain stable and converged deflections. In our finite element models, illustrated in Fig. 3, there are around 79920 elements and 33720 elements, 4 division of the minimum length, for the piezoactuator with and without a center mass, respectively. Results of the harmonic analysis to the piezoactuators are presented in Fig. 4, suggesting that the amplitude is significantly amplified when the actuators are excited at their resonant frequencies, especially for the thinner actuators, such as type A, and the center mass load of 3.6 g effectively results in a decrease of the resonant frequencies by more than half. A comparison concerning resonant frequencies and amplitudes between the analytical calculations and the FEM simulations is shown in Table 3, and it indicates that offsets of the resonant frequency and amplitude are within 6.5% and 8.6%, respectively.

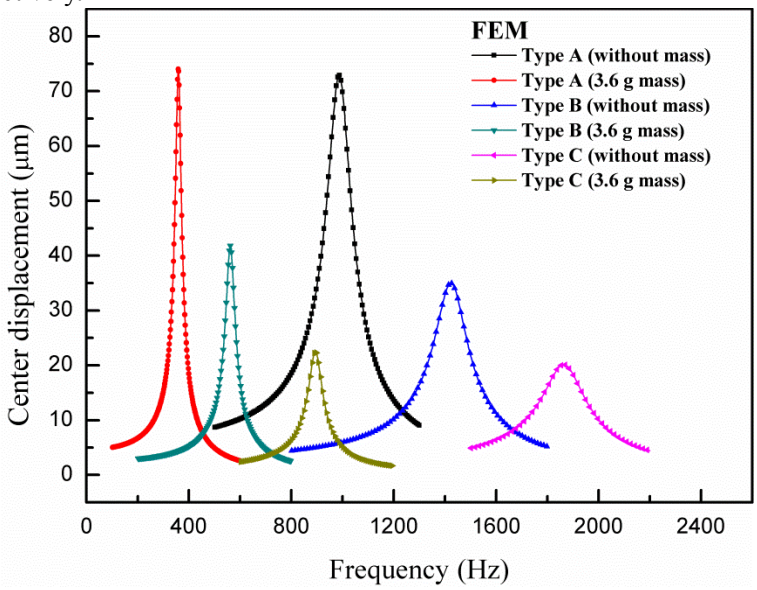

Fig. 4. Center displacement response of the piezoactuators for varying driven frequency under sinusoidal voltage of 20 V_{pp} through FEM

Table 3 FEM versus theoretical results for the three piezoactuators with and without 3.6 g mass

Type		Resonant frequency (Hz)		Center displacement (μm)	
		FEM	Analytical modeling	FEM	Analytical modeling
Type A (t=0.24 mm)	Without mass	986	962	72.1	68.4

Type A (t=0.24 mm)	3.6g mass	352	329	74	77.3
Type B (t=0.36 mm)	Without mass	1424	1431	35	32.3
	3.6 g mass	562	577	41.8	38.2
Type C (t=0.5 mm)	Without mass	1864	1924	20.1	21.8
	3.6 g mass	894	880	23.5	25.5

3.3 Experiments

Vibrations of the three types of commercially available circular piezoactuators both with and without a mass load were measured through a laser displacement sensor. The main instruments in the experiments consisted of a piezoactuator clamper, a signal generator, an oscilloscope to display the excitation signal, and a laser displacement sensor (LK-G30, resolution of 0.1 μm) to measure the deflection. The photograph and schematic of the experiments setup were shown in Fig. 5. The clamper was comprised of an upper part with an extended lip and a lower part with a grove to fit the actuator, and was designed to provide an edge-clamped boundary condition to the piezoactuators. The effective clamped radius of the actuators is 17.5 mm. The laser sensor was mounted on an adjusted support allowed it to measure the displacement of any point on the piezoactuator. The cylinder mass of 3.6 g was tightly bonded to the piezoactuator center through AB adhesive. The piezoactuators were excited by sinusoidal electric signals with the frequency varied up to 2.5 kHz while keeping voltage constant at 20 V_{pp}. The center displacement of the piezoactuators was measured at various frequencies and the resonance frequency was taken when the driven frequency yielded the highest displacement.

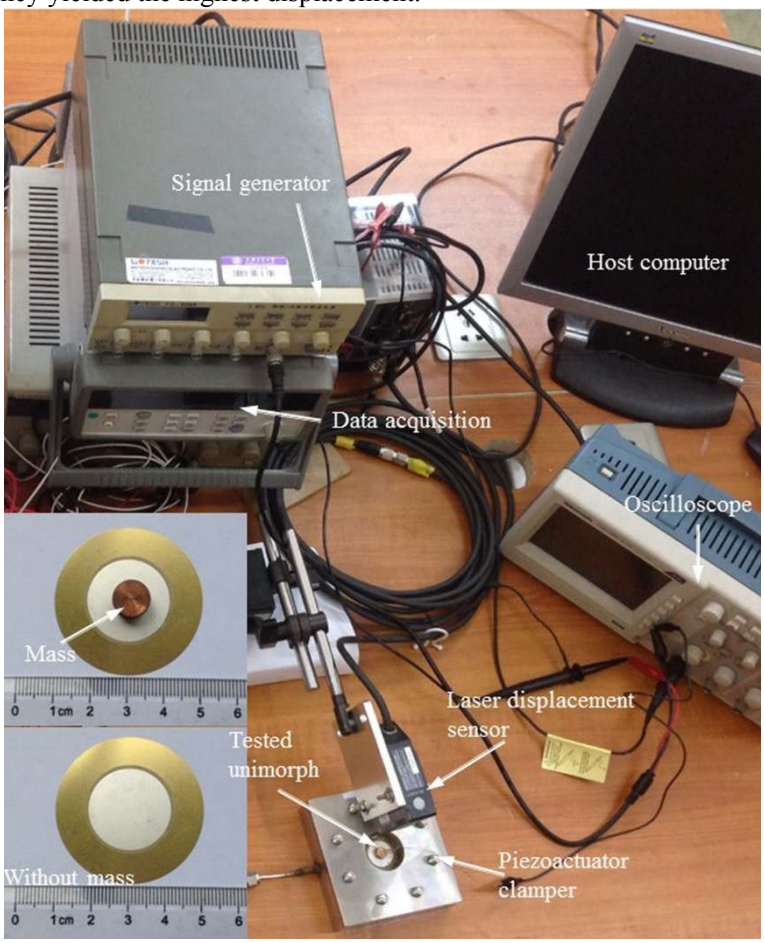

(a)

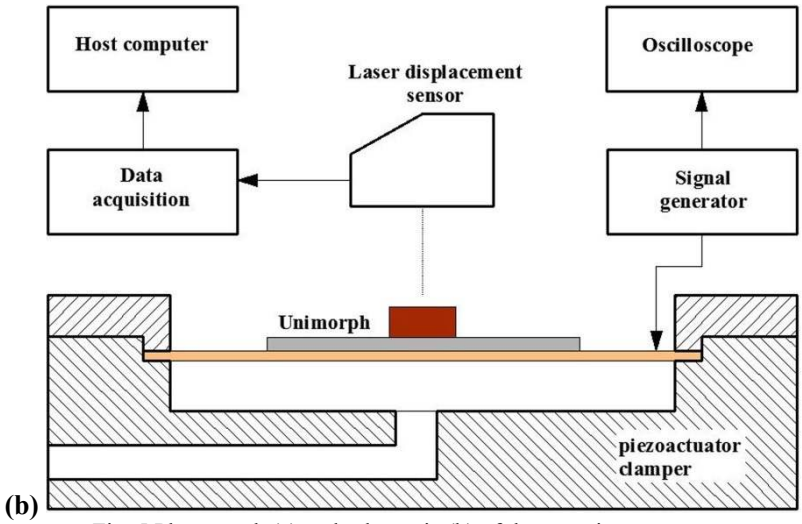

Fig. 5 Photograph (a) and schematic (b) of the experiments setup

The measured response of the center displacement, plotted in Fig. 6, highly agrees with the response from the FEM simulations, and also suggests that resonant excitation of the piezoactuators is effective in improving their vibration amplitude. Moreover, the resonant frequencies are significantly decreased due to the center mass load without weaken the amplitude; on the contrary the amplitude is slightly inched. The profiles of the three resonant piezoactuators are presented in Fig. 7, showing that the calculation ones match well with that from experimental measurements and the FEM simulations. The theoretical calculations are compared with the experimental measurements in details concerning the resonant frequencies and amplitudes, presented in Table 4, which indicates the deviations are within 10% and 7.6%, respectively.

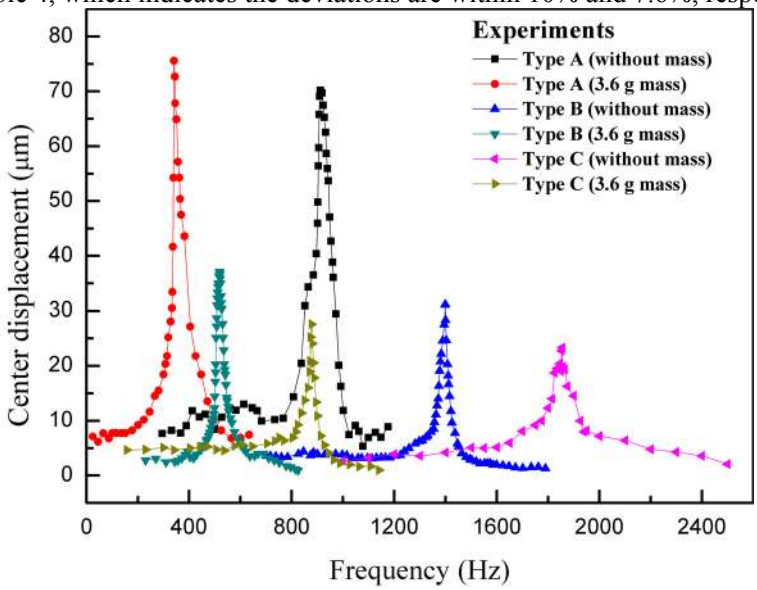

Fig. 6 Center displacement response of the tested piezoactuators for varying excitation frequency under sinusoidal voltage of 20 V_{pp}

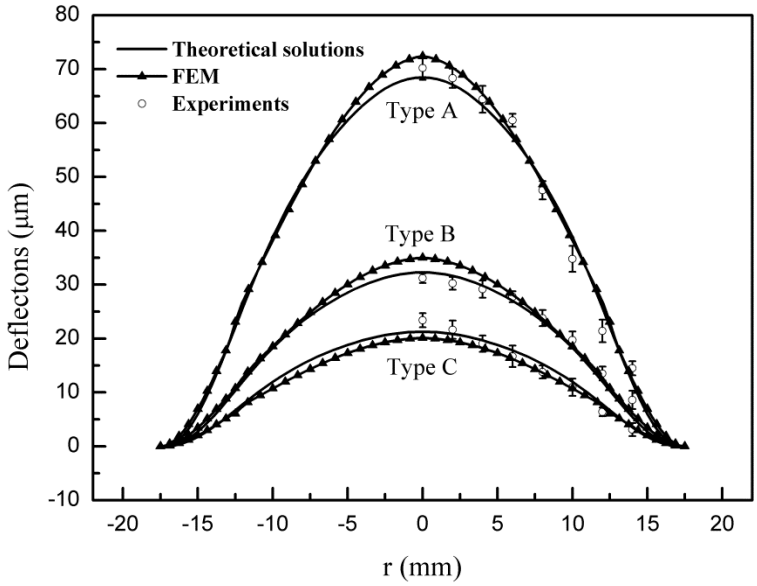

Fig. 7 Resonant profiles of the three piezoactuators without center mass

Table 4 Experimental results versus theoretical results

Type		Resonant frequency (Hz)		Center displacement (μm)	
		Experiment	Analytical modeling	Experiment	Analytical modeling
Type A	Without mass	912	962	70.2	68.4
	3.6g mass	341	329	75.6	77.3
Type B	Without mass	1399	1431	31.2	32.3
	3.6 g mass	519	577	37.1	38.2
Type C	Without mass	1855	1924	23.4	21.8
	3.6 g mass	878	880	27.6	25.5

4 Discussion of the resonant frequency

The analytical solution for the vibration behaviors of the circular diaphragm-type piezoactuators is highly valuable because it enable to design the piezoactuators quickly for specific operational requirements, especially in fluidic handling systems. According to the validation above, the theoretical calculation is accurate to predict the resonant frequency of the piezoactuators with and without the mass load. In this section, the investigation is further extended to different mass loads, geometric dimensions, and material properties based on the proposed equations.

4.1 Effects of the mass load

As discussed above, the mass load of 3.6 g at the diaphragm center are effective to decrease the resonant frequency of the piezoactuators, hence avoiding too high resonant frequency in many MEMS devices. Effects of different mass loads on the resonant frequency of the three piezoactuators are further discussed, shown in Fig. 8. The resonant frequency of the type B without mass load is 1431 Hz, while it decreases to 550 Hz when a mass load of 3.6 g is fixed at the diaphragm center, and decreases to 454 Hz with a mass load of 5.7 g. For the three types of actuators, the resonant frequency decreases sharply with the increasing added mass load when the load is less than 3.6 g; and when the mass load is over 3.6 g, the resonant frequency continues to decease with the increasing mass load, but in a much lower slope. This phenomenon denotes that the increasing mass load has a limit in decreasing the resonant frequency.

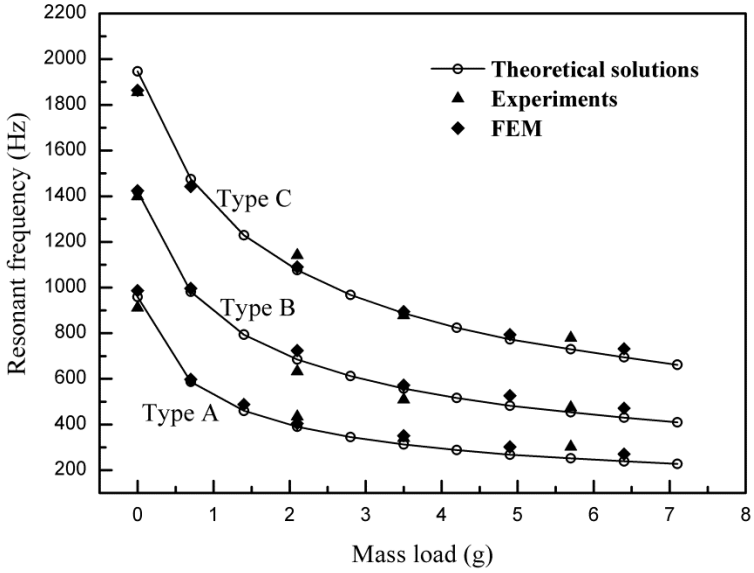

Fig. 8. Resonant frequency of the three piezoactuators varies with the added mass loads

4.2 Effects of the geometric dimensions

The dimensions of the diaphragm piezoactuator, especially for the radius ratio of the PZT layer to passive layer (r_2/r_1) and thickness of the passive layer (t_p), have significant impacts on the resonant frequencies as well. The piezoactuator of type B, both with and without a mass load, is employed to investigate the effects of r_2/r_1 and t_p on the resonant frequency. As shown in Fig. 9, without the mass load, the r_2/r_1 starts to affect the resonant frequency when it is over 0.75, and then the frequency increases rapidly with the increase of r_2/r_1. After the mass load is added, the resonant frequency slightly increases with the increase of r_2/r_1, but in a higher slope when the r_2/r_1 is over 0.83. Hence, a proper r_2/r_1 is helpful to avoid too high resonant frequency. As for the impacts of the passive layer thickness (t_p), presented in Fig. 10, the resonant frequency of the piezoactuator with and without mass load both linearly increases with the thickness, but the slope for the actuator with mass load is slightly lower.

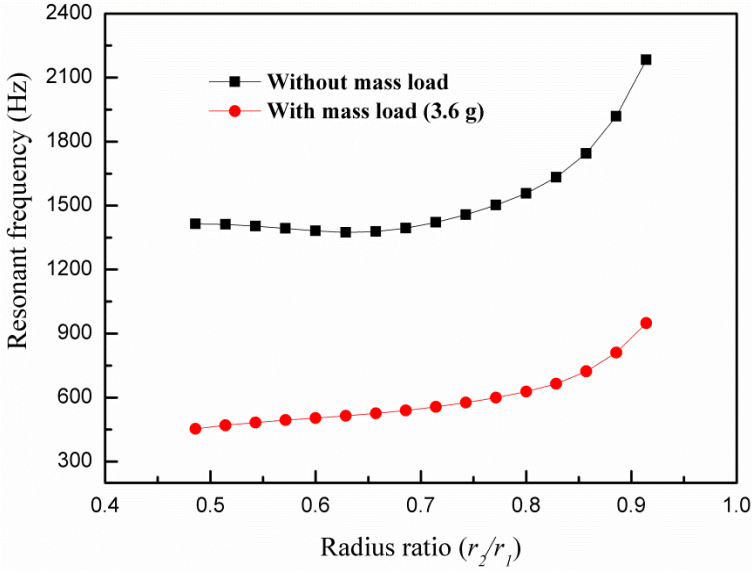

Fig. 9. Radius ratio (r_2/r_1) vs the resonant frequency

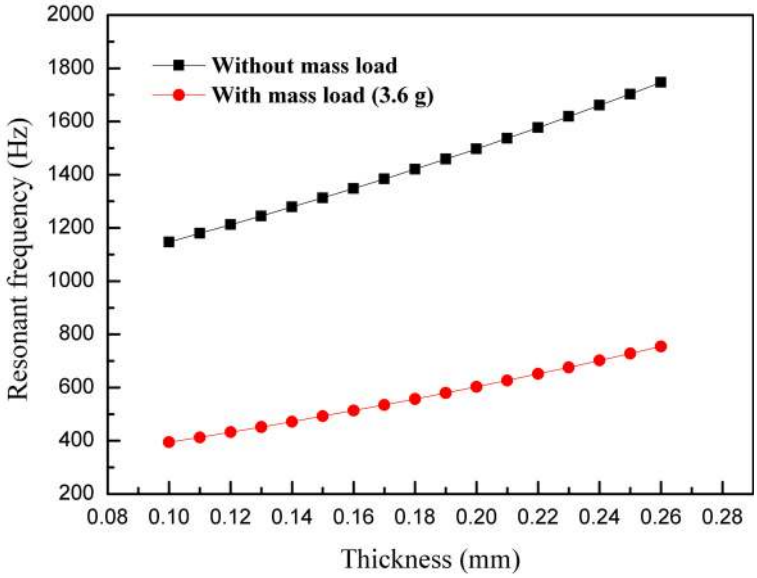

Fig. 10. Thickness of the passive layer (t_p) vs the resonant frequency

4.2 Effects of the passive layer material

The passive layer material is extended to other materials that have different Young's modulus and Poisson's ratio based on the analytical solution. According to the results, the resonant frequency varies within 3% both for the actuator with and without mass load while the Poisson's ratio ranges from 0.2 to 0.4, suggesting that the Poisson's ratio slightly affect the resonant frequency. As for the Young's modulus of the passive layer, shown in Fig. 11, the resonant frequency linearly increases with the increasing Young's modulus, which changed from 0.4 to 2 times that of the current one. Furthermore, the increasing slop for the actuator without the mass load is higher than that of the actuator with the mass load, indicating that the mass load on the diaphragm weakens the effects of the material Young's modulus.

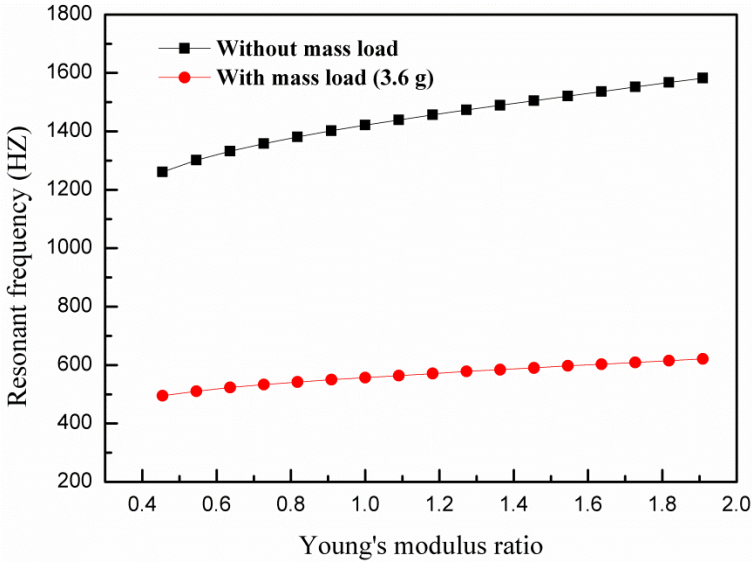

Fig. 11. Young's modulus of the passive layer vs the resonant frequency

5 Conclusion

An analytical solution on the vibration behaviors of the circular diaphragm-type piezoactuators is formulated based on the Hamilton principle and the Rayleigh-Ritz method, which enable to quickly analyze the piezoactuators resonantly working in the MEMS devices, such as the gas micropumps and ejectors. Moreover, a mass load has been fixed at the diaphragm center so as to avoid too high resonant frequency, and the method successfully decreases the resonant frequency by more than half. The solution can be applicable to the multilayer diaphragm-type piezoactuators according to the validation through FEM simulations and experimental

measurements.

The equations are convenient to be used for resonant analysis where the resonant frequency of the actuator can be calculated as explicit functions of the loads, geometric dimensions and material properties. From the discussion, a proper mass load on the diaphragm is highly effective to decrease the resonant frequency but the effect has a limit. Furthermore, the radius ratio (r_2/r_1) significantly increases the resonant frequency when r_2/r_1 is over 0.83, which needs to be avoided. As for the thickness of the passive layer (t_p), the resonant frequency linearly increases with the increase of t_p for the actuator with and without mass load. The Yong's modulus of the passive layer takes more important role than the Poisson's ratio in determining the resonant frequency, and the effect is weakened when the mass load is added.

Acknowledgments

The authors are grateful for the support of the National Science Foundation of China (Grant No. 51576123).

References

[1] B.D. Iverson, S.V. Garimella, Recent advances in microscale pumping technologies: a review and evaluation, Microfluidics and Nanofluidics, 5(2008) 145-74.

[2] C.H.C. D. A. Wang, Y. H. Hsieh, Z. X. Zhang, Analysis of an annular PZT actuator for a droplet ejector, Sensors and Actuators A: Physical, 137(2007) 8.

[3] N.-C. Tsai, C.-Y. Sue, Review of MEMS-based drug delivery and dosing systems, Sensors and Actuators A: Physical, 134(2007) 555-64.

[4] M. Deshpande, L. Saggere, An analytical model and working equations for static deflections of a circular multi-layered diaphragm-type piezoelectric actuator, Sensors and Actuators A: Physical, 136(2007) 673-89.

[5] R.W. Changki Mo, William S Slaughter, WilliamW Clark, Behaviour of a unimorph circular piezoelectric actuator, SMART MATERIALS AND STRUCTURES, 15(2006) 9.

[6] S. Li, S. Chen, Analytical analysis of a circular PZT actuator for valveless micropumps, Sensors and Actuators A: Physical, 104(2003) 151-61.

[7] J.S. Yoon, J.W. Choi, M.S. Kim, Y.-E. Yoo, D.-S. Choi, Studies on the performance characteristics and improvements of the piezoelectrically-driven micro gas compressors, Microelectronic Engineering, 86(2009) 2297-304.

[8] G. Perçin, Plate Equations for Piezoelectrically Actuated Flexural Mode Ultrasound Transducers, IEEE transactions on ultrasonics, ferroelectrics, and frequency control, 50(2003) 8.

[9] B.A. Selim, L.W. Zhang, K.M. Liew, Active vibration control of FGM plates with piezoelectric layers based on Reddy's higher-order shear deformation theory, Composite Structures, 155(2016) 118-34.

[10] M.R. Bai, R.L. Chen, C.Y. Chuang, C.S. Yu, H.L. Hsieh, Optimal design of resonant piezoelectric buzzer from a perspective of vibration-absorber theory, The Journal of the Acoustical Society of America, 122(2007) 1568.

[11] Q. Wang, Quek, S. T., Sun, C. T., Liu, X., Analysis of piezoelectric coupled circular plate, Smart Materials and Structures, 10(2001) 11.

[12] W.H. Duan, S.T. Quek, Q. Wang, Free vibration analysis of piezoelectric coupled thin and thick annular plate, Journal of Sound and Vibration, 281(2005) 119-39.

[13] S. Hosseini-Hashemi, M. Es'haghi, H. Rokni Damavandi Taher, An exact analytical solution for freely vibrating piezoelectric coupled circular/annular thick plates using Reddy plate theory, Composite Structures, 92(2010) 1333-51.

[14] L. Yao, Lu, L., Wang, Z., Zhu, W., Dai, Y., Exact solution of multilayered piezoelectric diaphragms, IEEE transactions on ultrasonics, ferroelectrics, and frequency control, 50(2003) 10.

[15] S. Zhao, Shi, Z., Xiang, H., The primary resonance of laminated piezoelectric rectangular plates, IEEE transactions on ultrasonics, ferroelectrics, and frequency control, 56(2009) 8.

[16] M. Olfatnia, T. Xu, L.S. Ong, J.M. Miao, Z.H. Wang, Investigation of residual stress and its effects on the vibrational characteristics of piezoelectric-based multilayered microdiaphragms, Journal of Micromechanics and Microengineering, 20(2010) 015007.

[17] M. Olfatnia, V.R. Singh, T. Xu, J.M. Miao, L.S. Ong, Analysis of the vibration modes of piezoelectric circular microdiaphragms, Journal of Micromechanics and Microengineering, 20(2010) 085013.

[18] L.T. Gomes, Effect of damping and relaxed clamping on a new vibration theory of piezoelectric diaphragms, Sensors and Actuators A: Physical, 169(2011) 12-7.

[19] S. Kaviani, M. Bahrami, A.M. Esfahani, B. Parsi, A modeling and vibration analysis of a piezoelectric micro-pump diaphragm, Comptes Rendus Mécanique, 342(2014) 692-9.

[20] M.B. Amir Monemian Esfahani, Vibration analysis of a circular thin polymeric piezoelectric diaphragm with fluid interaction, Int J Mech Mater Des, 12(2016) 11.

[21] M.B. Amir Monemian Esfahani, Seyed Reza Ghaffarian Anbarani, Forced vibration analysis of a viscoelastic polymeric piezoelectric microplate with fluid interaction, Micro & Nano Letters, 11(2016) 7.

[22] Q.S. Pan, L.G. He, F.S. Huang, X.Y. Wang, Z.H. Feng, Piezoelectric micropump using dual-frequency drive, Sensors and Actuators A: Physical, 229(2015) 86-93.

[23] M. Olfatnia, Z. Shen, J.M. Miao, L.S. Ong, T. Xu, M. Ebrahimi, Medium damping influences on the resonant frequency and quality factor of piezoelectric circular microdiaphragm sensors, Journal of Micromechanics and Microengineering, 21(2011) 045002.

[24] R. Andosca, T.G. McDonald, V. Genova, S. Rosenberg, J. Keating, C. Benedixen, et al., Experimental and theoretical studies on MEMS piezoelectric vibrational energy harvesters with mass loading, Sensors and Actuators A: Physical, 178(2012) 76-87.
[25] M. Arik, S.M. Zurn, A. Bar-Cohen, D.L. Polla, Design, fabrication, and characterization of thin film PZT membranes for high flux electronics cooling applications, Smart Materials and Structures, 14(2005) 1239-49.
[26] C. Qifeng, L. Chengliang, X.F. Zha, Modeling and Numerical Analysis of a Circular Piezoelectric Actuator for Valveless Micropumps, Journal of Intelligent Material Systems and Structures, 19(2007) 1195-205.
[27] S.P. Timoshenko, Sergius Woinowsky-Krieger, Theory of plates and shells, McGraw-hill1959.
[28] H. Ma, X. Gao, J. Reddy, A microstructure-dependent Timoshenko beam model based on a modified couple stress theory, Journal of the Mechanics and Physics of Solids, 56(2008) 3379-91.
[29] Z. Ji, J.W. Zu, METHOD OF MULTIPLE SCALES FOR VIBRATION ANALYSIS OF ROTOR SHAFT SYSTEMS WITH NON-LINEAR BEARING PEDESTAL MODEL, Journal of Sound and Vibration, 218(1998) 293-305.